Journal of Solid State Chemistry 181 (2008) 3194–3199

Contents lists available at ScienceDirect

Journal of Solid State Chemistry

journal homepage: www.elsevier.com/locate/jssc

Phase separation, cation ordering and nano-structural complexities in $Nd_{2/3-x}Li_{3x}TiO_3$ with $x = 0.14$

J.B. Lu, H.X. Yang, Z.A. Li, C. Ma, H.L. Shi, L.J. Zeng, J.Q. Li *

Beijing National Laboratory for Condensed Matter Physics, Institute of Physics, Chinese Academy of Sciences, Beijing 100190, China

ARTICLE INFO

Article history:
Received 24 June 2008
Received in revised form
5 August 2008
Accepted 12 August 2008
Available online 22 August 2008

Keywords:
Transmission electron microscopy
Perovskite
Phase separation
Cation ordering
Superstructure

ABSTRACT

Transmission electron microscopy (TEM) investigations on $Nd_{2/3-x}Li_{3x}TiO_3$ with $x = 0.14$ reveal a rich variety of structural features in the samples prepared under different conditions, such as superstructures, anti-phase domains, and nano-chessboard structures. Our careful analysis shows that these structural phenomena can be fundamentally understood as the combination of structural effects of (Nd, Li)-ordering along the $\langle 001 \rangle_p$ direction and the spinodal decomposition along the $\langle 100 \rangle_p/\langle 010 \rangle_p$ direction. The coexistence of phase separation and cation ordering can lead to visible nano-structural complexities in many crystals, as the typical results, the regular lamella structure, nano-chessboard structures and anti-phase boundaries have been extensively studied.

1. Introduction

Materials with the perovskite-related structure of formula $RE_{2/3-x}Li_{3x}TiO_3$ (RE = La, Pr, Nd) have attracted a great deal of interest owing to their high value of ionic conductivity and the possible applications as solid electrolyte in all-solid-state lithium batteries [1–8]. In 1995, Robertson et al. performed a series of investigations about the physical and structural properties of the $Li_{0.5-3x}RE_{0.5+x}TiO_3$ (RE = La, Nd) materials and showed the phase diagrams and polymorphs for both solid solutions. Three polymorphs β, α, A ($0.025 < x < 0.13$) in the La system and four polymorphs β, α', A and C ($0.016 < x < 0.12$) in the Nd system [9] were determined depending on the temperature and composition. The microstructure properties of the $Li_{0.5-3x}Nd_{0.5+x}TiO_3$ ($0.016 < x < 0.12$) samples were studied by electron diffraction and high-resolution transmission electron microscopy (HRTEM) observations [10]. The results suggested that β and α' have the same lattice structure and the main diffraction peaks can be well indexed to a diagonal perovskite cell with lattice parameters of $\sqrt{2}a_p \times \sqrt{2}a_p \times \sqrt{22}a_p$, where a_p is the basic cubic perovskite cell parameter. Recently, Guiton and Davies [11] found that the spontaneous phase separation in $Nd_{2/3-x}Li_{3x}TiO_3$ ($0.047 < x < 0.151$) materials could result in the ordered (001) layers recognizable as Li-rich square domains separated by Li-poor boundaries. Nevertheless, because of the complexity in the A-site deficient perovskites, a variety of defect structures, ordered states and local structure distortions have been widely examined in previous publications [12–15]. In this paper, we will report on microstructure features of $Nd_{2/3-x}Li_{3x}TiO_3$ with $x = 0.14$ prepared under different conditions. In the sample quenched from 1000 °C into liquid nitrogen, TEM observations clearly demonstrate the presence of a $2c_p$ superstructure along $\langle 001 \rangle_p$ direction. Moreover, the spinodal decomposition as observed in many samples could yield complicated nano-scale phase separation, as a result, one-dimensional stripes pattern and two-dimensional chessboard pattern often appear in $Nd_{2/3-x}Li_{3x}TiO_3$ materials.

2. Experimental

Polycrystalline materials with a nominal composition $Nd_{2/3-x}Li_{3x}TiO_3$ with $x = 0.14$ were prepared by the method as described by Robertson et al. [9]. The materials of Li_2CO_3 (99.9%), TiO_2 (99.9%) and Nd_2O_3 (99.9%) were first dried, respectively, overnight at 400, 600 and 1000 °C prior to weighting. The mixture was ground, pressed into pellets, covered with powder of the same composition to avoid Li loss and fired in air at 1100 °C for 12 h and followed by further grinding, repelleting and refiring at 1300 °C for another 12 h. At the end of the second step, the samples were cooled to 600 °C at a rate of 30–100 °C/h before removing out of the furnace. It is noted that the cooling rate can evidently affect the microstructure features of the products as revealed in TEM observations; samples prepared with a cooling

* Corresponding author. Fax: +86 10 6256 1422.
E-mail address: LJQ@aphy.iphy.ac.cn (J.Q. Li).

0022-4596/$ - see front matter © 2008 Elsevier Inc. All rights reserved.
doi:10.1016/j.jssc.2008.08.016

rate of 100 °C/h (sample B) were govern by the one-dimensional stripes and samples with a rate of 50 °C/h (sample C) or slower were governed by two-dimensional nano-chessboard patterns. Moreover, regular patterns often appear in the sample annealed at 800 °C for 30 h. In order to investigate the microstructure features of Li-ordering, some materials (sample A) were quenched from 1000 °C into liquid nitrogen.

Structural phase identification was carried out by powder X-ray diffraction (XRD) using a Rigaku diffractometer with Cu$K\alpha$ radiation. The microstructure properties and chemical composition of the as-grown samples were analyzed on a Philips XL30 scanning electron microscopy (SEM). TEM investigations were performed on a Tecnai F20 operating at a voltage of 200 kV. Specimens for TEM observations were polished mechanically with a Gatan polisher to a thickness of around 50 μm and then ion-milled by a Gatan-691 PIPS ion miller. In addition, we also prepared some thin samples for electron diffraction experiments simply by crushing the bulk material into fine fragments, which were then supported by a copper grid coated with a thin carbon film.

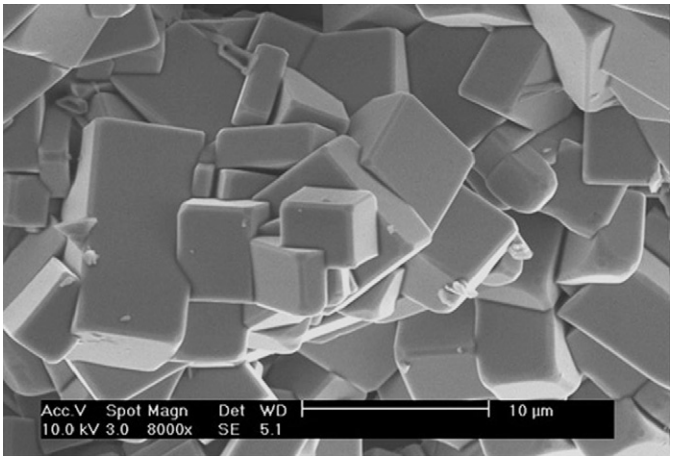

Fig. 1. SEM image of sample B showing the large regular crystals in the as-grown materials.

3. Results and discussion

The as-synthesized products were first analyzed by using a SEM. Fig. 1 shows a typical SEM image of sample B prepared at a cooling rate of 100 °C/h, illustrating that the sample consists of a large crystal grain with a size of 5–10 μm. These crystals in general have regular square shapes which are essentially in connection with the crystal symmetry for the average unit cell, and further investigations reveal that these regular crystals contain a variety of structural inhomogeneity and complex defects as discussed in the following context. The SEM images of samples A and C are similar to those of sample B. XRD experiment revealed that $Nd_{2/3-x}Li_{3x}TiO_3$ with $x = 0.14$ prepared under different conditions possesses a perovskite-type structure. The major diffraction peaks in the spectra can be well indexed to tetragonal phase with $a = 3.8245$ Å, $c = 7.6809$ Å (JCPDS file 46-0464). Due to a small amount of Li loss during high-temperature sintering, some other weak peaks can be assigned to the monoclinic $Nd_2Ti_2O_7$ with a space group of $P2_1$ and the lattice parameters of $a = 13.008$ Å, $b = 5.4648$ Å, and $c = 7.679$ Å.

It is commonly noted in the previous literatures that the $Nd_{2/3-x}Li_{3x}TiO_3$ samples prepared under different conditions show up remarkable different structural features [9,10]. The high-temperature annealing as well as liquid nitrogen quenching

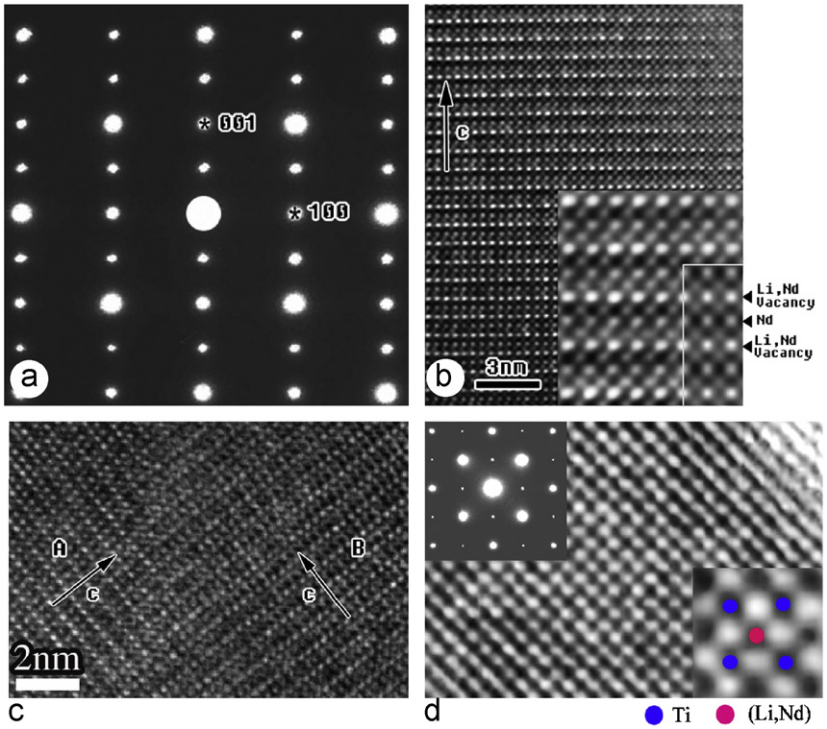

Fig. 2. Electron diffraction pattern and high-resolution TEM image of sample A: (a) the $[010]_p$ zone-axis diffraction pattern and (b) the $[010]_p$ zone-axis HRTEM image showing the presence of $2c_p$ superstructure along the $\langle 001 \rangle_p$ direction. Inset shows an HRTEM image with large magnification illustrating atomic structures. A simulated image with the defocus value of −24 nm and thickness of 3 nm is superimposed on the inset image, (c) HRTEM image showing a 90°-domain structure, and (d) the HRTEM image along the $[001]_p$ zone axis showing the perovskite atomic structure, the insets show the corresponding electron diffraction pattern and the magnified HRTEM image, respectively.

treatments often yields visible structural modifications. For instance, the notable nano-chessboard structure in $Nd_{2/3-x}Li_{3x}TiO_3$ originates from the periodic two-dimensional nanometer-scale phase separation [11,16], and superstructure phases arise from La vacancy order in $La_{0.61}Li_{0.18}TiO_3$ quenched from 1600 K to liquid nitrogen [17]. We therefore carried out extensive investigations on the microstructure properties of a series of materials prepared under different conditions.

It is noted that the Li^+ ions and vacancies existing in $RE_{2/3-x}Li_{3x}TiO_3$ materials could result in certain notable structural features as revealed in our TEM observations. The experimental analysis demonstrated that the rare-earth ions and vacancies ordered within alternate (001) layer in the perovskites always lead to doubling of the unit-cell c parameter, and the well-defined superstructure phase is often observed in the sample quenched into liquid nitrogen from 1000 °C. Fig. 2(a) and (b) show an electron diffraction pattern and an HRTEM image taken along the $[010]_p$ zone-axis direction, demonstrating the presence of the $2c_p$ superstructure in the quenched sample A as reported in previous literature [9]. Careful investigations along several main zone axes suggest that the unit cell of the quenched crystal can be written as $a_p \times a_p \times 2a_p$ which is similar to the β-phase as reported by Robertson et al. [9], where a_p is the basic cubic perovskite cell parameter. This ordered state in La(Li)TiO_3 materials is considered to originate from the alternation of fully occupied La (001) layers and partially occupied mixed layers comprised of Li, La and vacancy [11]. The inset of Fig. 2(b) shows a large magnification HRTEM image, clearly displaying the atomic structural features of the superstructure phase. This image was obtained from a thin region of crystal under the defocus value at around the Scherzer

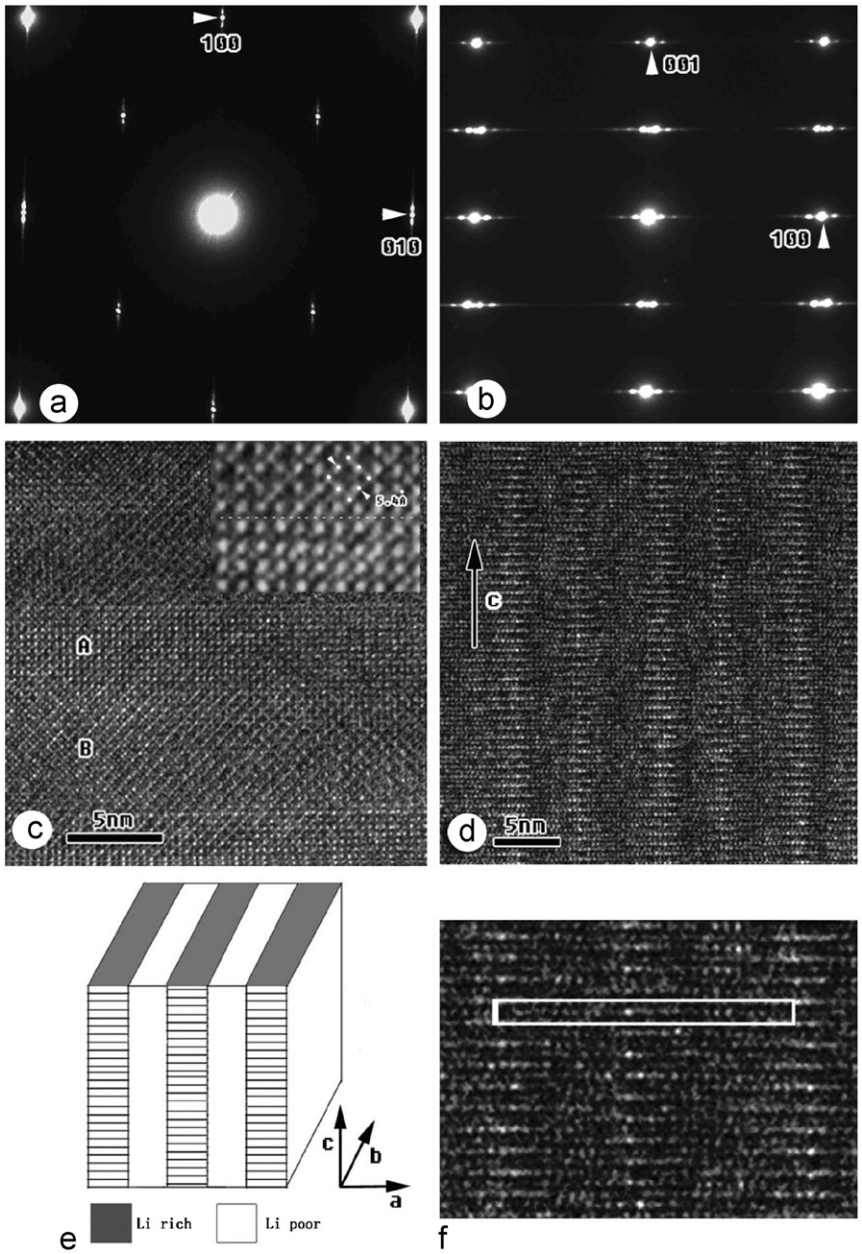

Fig. 3. Electron diffraction patterns of sample B taken along (a) the $[001]_p$ zone axis and (b) $[010]_p$ zone axis, (c) HRTEM image taken along the $[001]_p$ zone axis, the inset illustrating a clear boundary between $\sqrt{2}a_p \times \sqrt{2}a_p$ and $a_p \times a_p$ phases, (d) HRTEM image taken along the $[010]_p$ zone axis, (e) schematic representation of a crystal with one-dimensional micro-domain structure from phase separation, and (f) an HRTEM image of the $[010]_p$ zone axis illustrating the anti-phase relation between Li-rich domains.

defocus (~−36 nm). The metal atom positions are therefore recognizable as dark dots. Theoretical simulations on this ordered state revealed an alternative fully occupied Nd (001) layer, partially occupied mixed layers containing Nd and Li cations, and vacancies. A simulated image with a defocus value of −24 nm and the thickness of 3 nm is superimposed on the inset image of Fig. 2(b) in good agreement with the experimental one. Fig. 2(c) shows a 90°-domain structure frequently observed in sample A. The superstructures in areas A and B are rotated by 90° with respect to each another. TEM observations along *c*-axis direction often show a well-defined perovskite structure as illustrated in Fig. 2(d).

In addition to the (Li, Nd)-ordered state as mentioned above, a rich variety of microstructure phenomena are also observed in the $Nd_{2/3-x}Li_{3x}TiO_3$ compounds, such as the nano-scale chessboard superlattice [11], complex two-dimensional arrays arising from compositional modulations, twinning lamella and anti-phase boundaries. In order to understand the fundamental properties of the structural phenomena, we have performed a series of TEM observations on several typical samples, the experimental results suggest that the formation of the periodic one/two-dimensional nanometer phase separation is essentially driven by spinodal decomposition. In principle, spinodal decomposition should be expected to occur by quenching from above a critical temperature and aging at a temperature within the spinodal region, it is also possible to study the kinetics of the process by slower cooling. There has been a tendency to employ morphology as a mark of spinodal decomposition. For example, a specific repetitive spacing or mutual connectivity between the conjugate product phases has been used to confirm the operation of the process [18]. In order to

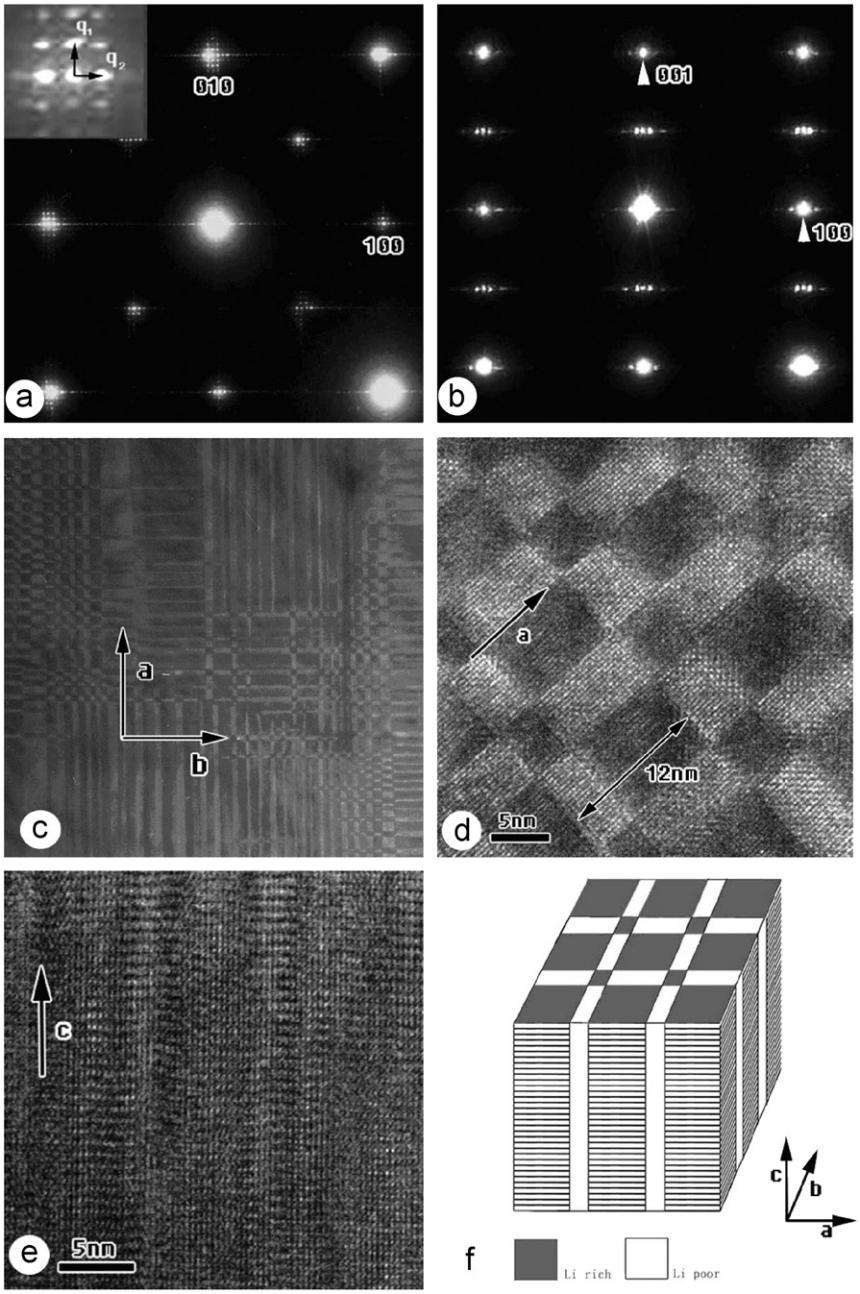

Fig. 4. (a) Electron diffraction pattern of sample C taken along the $[001]_p$ zone axis, the inset shows the magnified superlattice spots around ($\bar{1}00$) spot, (b) electron diffraction pattern taken along the $[010]_p$ zone axis, (c) bright-field TEM image corresponding to (a), (d) the $[001]_p$ zone-axis HRTEM image showing the two-dimensional nano-domains, (e) the $[100]_p$ zone-axis HRTEM image, and (f) schematic representation of a crystal with two-dimensional micro-domain structure.

capture an earlier stage of the decomposition process and to minimize solute clustering during quenching, liquid-quenching techniques were used.

Fig. 3 shows the typical electron diffraction patterns and HRTEM images taken from sample B. It is recognizable that in addition to the basic diffraction spots a series of weak satellite spots follow each main spot. This fact directly suggests a structural modulation appearing along the $\langle 100 \rangle_p$ direction. Careful observations revealed that the satellite spots often show up visible streaking (or diffuse satellite reflection streaks parallel to $g_{[100]_p}$) and multi-mode behaviors, suggesting complex microstructure features of present materials. In general, the modulation has a wave vector q between $a^*/15$ and $a^*/35$. To characterize the fundamental structural feature in connection with the observed pseudo-periodic modulation, we have carried out an extensive study on as-synthesized sample B. Fig. 3(c) shows an HRTEM image taken along $[001]_p$ zone-axis direction, illustrating the presence of one-dimensional lamella structure with a pseudo-periodicity of about 11 nm in good agreement with the data obtained from electron diffraction. In particular, another most streaking structural feature revealed in the high-resolution image of Fig. 3(c) is the coexistence of structural domains with $a_p \times a_p$ and $\sqrt{2}a_p \times \sqrt{2}a_p$ structures, as illustrated, respectively, in the areas A and B. These results likely suggest a periodic intergrowth state of Li-poor and Li-rich phases, and the $\sqrt{2}a_p \times \sqrt{2}a_p$ structure is clearly visible in Li-rich areas. Actually, either structural analysis or Z-contrast imaging by using high angle annular dark-field scanning TEM (STEM) can demonstrate that the lamella structures are in connection with a phase separation. Careful analysis of the TEM results suggests that images obtained from relative thick areas often reveal complex strain contrast in association with nano-domain structures. On the other hand, the clear domain boundaries appear in thin areas as shown in the inset of Fig. 3(c), illustrating a clear boundary between $\sqrt{2}a_p \times \sqrt{2}a_p$ and $a_p \times a_p$ phases. Fig. 3(d) shows images corresponding to the diffraction pattern in Fig. 3(b), illustrating the structural feature observed along $[010]_p$ zone-axis direction. It again shows a pseudo-periodic lamella structure contrast corresponding to a structural modulation along a-axis direction. Careful investigations suggest that both ordered structures in Fig. 3(c) and (d) represent aspects of the same structural features, as schematically illustrated in a brief model of Fig. 3(e).

Careful study on the local structural features reveals that the well-defined c-doubling superstructure can be only observed in the Li-rich lamella regions. Fig. 3(f) shows a TEM image of the a–c plane with larger magnification. Despite plenty of structural inhomogeneity, one can observe clear anti-phase structure among the Li-rich domains. They actually show a remarkable tendency to form a body (face)-centered stacking along the c-axis. Such an arrangement minimizes the Coulomb repulsion between the ordered Li-ions. The white box outlines an approximate large unit cell. The body centering is only approximate because of the influence of a variety of structural reasons, such as local defects, inhomogeneity and strains. Careful analysis of the most visible contrast in the present image demonstrates that the APB relationship occurs in (Li, Nd) layers.

Fig. 4 shows the experimental TEM data illustrating the major structural feature of sample C prepared by a slower cooling rate of 50 °C/h, it is recognizable that, in contrast with the data of sample B, this sample often contains complex two-dimensional regular domain structures. Fig. 4(a) and (b) shows, respectively, the electron diffraction pattern taken along $[001]_p$ and $[010]_p$ zone axis. In addition to the basic reflections, it can be clearly seen that two sets of superstructure reflections appear around $(h00)_p$, $(0k0)_p$ and $(\frac{11}{22}0)_p$ spots within an approximately rectangular configuration. Careful analysis suggests this two-dimensional modulation has the periods of about 12 nm along both $g_{[100]_p}$ and $g_{[010]_p}$ directions. Fig. 4(c) shows a bright-field TEM image corresponding to the diffraction pattern of Fig. 4(a), demonstrating the presence of two-dimensional lamella state in our sample. Moreover, according to our TEM data obtained on a series of samples, the two-dimensional lamella states in certain samples show up as perfect nano-chessboard superlattices; however, the nano-chessboard structures exhibit certain notable features in orientation different from the data reported by Guiton and Davies [11]. Fig. 4(d) displays the HRTEM image taken along the $[001]_p$ zone axis, illustrating nano-chessboard superlattice observed in our samples. The domain structure goes along the $\langle 100 \rangle_p / \langle 010 \rangle_p$ direction in contrast with the $\langle 110 \rangle_p$ direction as reported by Guiton and Davies [11]. In order to understand the microstructure feature along the c-axis direction, we have also performed high-resolution TEM observations along other relevant zone-axis directions as typically shown in Fig. 4(e), it is notable that the anti-phase domain structure in association with cation ordering is much more complex than that observed in sample B. Fig. 4(f) shows a schematic structural model illustrating the domain structural properties observed in sample C.

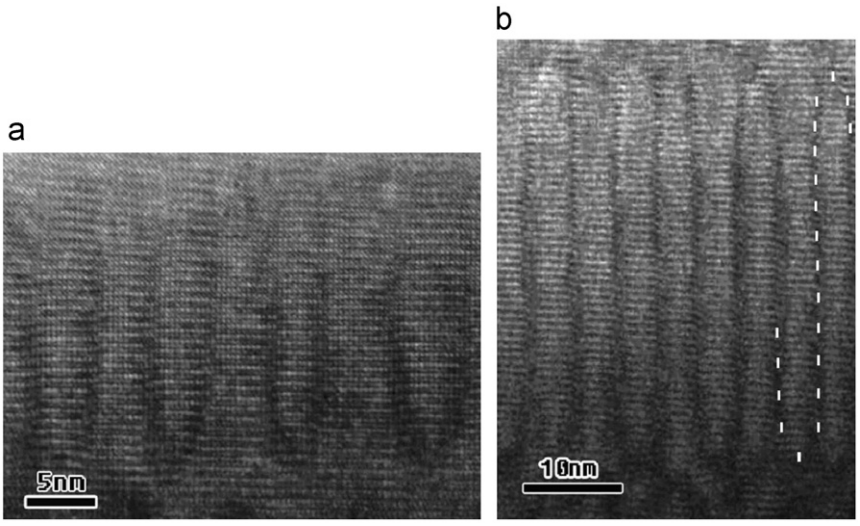

Fig. 5. Nano-structural complexities arising from the phase separation and (Li, Nd)-ordering in sample C: (a) a cycle-like pattern and (b) a wave-like pattern.

In addition to the one- and two-dimensional parallel lamella structure mentioned above, our TEM investigations also show that the phase separation could also result in complex microstructure patterns in $Nd_{2/3-x}Li_{3x}TiO_3$ (sample C), e.g. the cycle- and wave-like patterns as shown in Fig. 5(a) and (b). These images are all obtained along the $[010]_p$ zone-axis direction and demonstrate the $2c_p$ superstructure along the *c*-axis direction in Li-rich areas. It is recognizable that the spinodal decomposition in these regions results in the circle- or wave-like routes and notable structural distortions in vicinity areas of the domain boundaries.

4. Conclusions

The microstructure features of the samples $Nd_{2/3-x}Li_{3x}TiO_3$ with $x = 0.14$ obtained under different preparation conditions have been studied by means of transmission electron microscopy. In the sample quenched into liquid nitrogen from 1000 °C, the *c*-doubling superstructure commonly occurs along the $\langle 001 \rangle_p$ direction, this ordered state is considered to originate from (Nd, Li)-ordering along the *c*-axis direction. In the samples cooled at the rates of 100 and 50 °C/h, the spinodal decomposition features occur mostly along the $\langle 100 \rangle_p/\langle 010 \rangle_p$ direction governed by the one (or two)-dimensional stripes and nano-scale chessboard patterns. Our careful analysis shows that these remarkable structural phenomena arise commonly from the phase separations and (Li, Nd) ordering in the Li-rich regions. In addition to the one- and two-dimensional regular lamella structure, the spinodal decomposition could also result in a variety of nano-structural complexities, such as the circle- or wave-like patterns. These microstructure results could be beneficial for researchers to understand the fundamental structural properties of $Nd_{2/3-x}Li_{3x}TiO_3$ materials and to design new functional materials such as new Li-ion conductors and the assembly of nano-scale materials.

Acknowledgments

This work is supported by the National Science Foundation of China, the Knowledge Innovation Project of the Chinese Academy of Sciences, and the 973 projects of the Ministry of Science and Technology of China.

References

[1] Y. Inaguma, C. Liquan, M. Itoh, T. Nakamura, T. Uchida, H. Ikuta, M. Wakihara, Solid State Commun. 86 (1993) 689–693.
[2] M. Morales, A.R. West, Solid State Ionics 91 (1996) 33–43.
[3] M. Yashima, M. Itoh, Y. Inaguma, Y. Morii, J. Am. Chem. Soc. 127 (2005) 3491–3495.
[4] J. Ibarra, A. Várez, C. León, J. Santamaría, L.M. Torres-Martínez, J. Sanz, Solid State Ionics 134 (2000) 219–228.
[5] J.M.S. Skakle, G.C. Mather, M. Morales, R.I. Smith, A.R. West, J. Mater. Chem. 5 (11) (1995) 1807–1808.
[6] M. Catti, M. Sommariva, R.M. Ibberson, J. Mater. Chem. 17 (2007) 1300–1307.
[7] Q.N. Pham, C. Bohnke, O. Bohnke, Surf. Sci. 572 (2004) 375–384.
[8] S. Stramare, V. Thangadurai, W. Weppner, Chem. Mater. 15 (2003) 3974–3990.
[9] A.D. Robertson, S.G. Martin, A. Coats, A.R. West, J. Mater. Chem. 5 (9) (1995) 1405–1412.
[10] S. García-Martín, F. García-Alvarado, A.D. Robertson, A.R. West, M.A. Alario-Franco, J. Solid State Chem. 128 (1997) 97–101.
[11] B.S. Guiton, P.K. Davies, Nat. Mater. 6 (2007) 586–591.
[12] S. García-Martín, M.Á. Alario-Franco, J. Solid State Chem. 148 (1999) 93–99.
[13] M.A. Alario-Franco, I.E. Grey, J.C. Joubert, H. Vincent, M. Labeau, Acta Crystallogr. A 38 (1982) 177–186.
[14] M. Labeau, I.E. Grey, J.C. Joubert, H. Vincent, M.A. Alarío-Franco, Acta Crystallogr. A 38 (1982) 753–761.
[15] J. Sanz, A. Varez, J.A. Alonso, M.T. Fernandez, J. Solid State Chem. 177 (2004) 1157–1164.
[16] P.M. Woodward, Nat. Mater. 6 (2007) 549–551.
[17] A. Varez, Y. Inaguma, M.T. Fernández, J.A. Alonso, J. Sanz, Chem. Mater. 15 (2003) 4637–4641.
[18] A.M. Alper, Phase Diagrams: Materials Science and Technology, vol. 5, Academic Press, New York, 1978, pp. 127–184.